HHS Public Access

Author manuscript

Circulation. Author manuscript; available in PMC 2015 October 21.

Published in final edited form as:

Circulation. 2014 October 21; 130(17): 1493–1504. doi:10.1161/CIRCULATIONAHA.114.011096.

CD82 Restrains Angiogenesis by Altering Lipid Raft Clustering and CD44 Trafficking in Endothelial Cells

Quan Wei, MD[1,2], **Feng Zhang, PhD**[1], **Mekel M. Richardson, PhD**[1], **Nathan H. Roy, PhD**[3], **William Rodgers, PhD**[1], **Yuechueng Liu, PhD**[1], **Wenyuan Zhao, PhD**[4], **Chenying Fu, PhD**[1], **Yingjun Ding, MD**[1,5], **Chao Huang, MS**[1], **Yuanjian Chen**[4], **Yao Sun, PhD**[4], **Lexi Ding, MD**[1], **Yang Hu, PhD**[1], **Jianxing Ma, PhD**[1], **Michael E. Boulton, PhD**[6], **Satish Pasula, PhD**[7], **Jonathan D. Wren, PhD**[7], **Satoshi Tanaka, PhD**[8], **Xiaolin Huang, MD**[5], **Markus Thali, PhD**[3], **Günter J. Hämmerling, PhD**[8], and **Xin A. Zhang, MD**[1]

[1]University of Oklahoma Health Science Center, Oklahoma City, OK

[2]West China Hospital, Sichuan University, Chengdu, China

[3]University of Vermont, Burlington, VT

[4]University of Tennessee, Memphis, TN

[5]Tongji Hospital, Wuhan, China

[6]Indiana University, Indianapolis, IN

[7]Oklahoma Medical Research Foundation, Oklahoma City, OK

[8]German Cancer Research Center, Heidelberg, Germany

Abstract

Background—Angiogenesis is crucial for many pathological processes and becomes a therapeutic strategy against diseases ranging from inflammation to cancer. The regulatory mechanism of angiogenesis remains unclear. Although tetraspanin CD82 is widely expressed in various endothelial cells (ECs), its vascular function is unknown.

Methods and Results—Angiogenesis was examined in *Cd82-null* mice with *in vivo* and *ex vivo* morphogenesis assays. Cellular functions, molecular interactions, and signaling were analyzed in *Cd82-null* ECs. Angiogenic responses to various stimuli became markedly increased upon *Cd82* ablation. Major changes of *Cd82-null* ECs were enhanced migration and invasion, likely resulting from the upregulated expression of cell adhesion molecules (CAMs) such as CD44 and integrins at the cell surface and subsequently elevated outside-in signaling. Gangliosides, lipid raft clustering, and CD44-membrane microdomain interactions were increased in the plasma membrane of *Cd82-null* ECs, leading to less clathrin-independent endocytosis and then more surface presence of CD44.

Correspondence: Xin A. Zhang, MD, University of Oklahoma Health Science Center, BRC1474, 975 10th Street, Oklahoma City, OK 73104, Phone: 405-271-8001, Fax: 405-271-2141, xin-zhang-1@ouhsc.edu.

Conflict of Interest Disclosures: None.

Conclusions—Our study reveals that CD82 restrains pathological angiogenesis by inhibiting EC movement, lipid raft clustering and CAM trafficking modulate angiogenic potential, and the perturbation of CD82-ganglioside-CD44 signaling attenuates angiogenesis.

Keywords

tetraspanin; membrane microdomain; cell migration; endocytosis; angiogenesis

Introduction

Vascular morphogenesis includes vasculogenesis and angiogenesis[1]. Both involve coordinated EC proliferation, EC migration, branching, and tube formation[2]. Deregulated vascular morphogenesis and pathological angiogenesis contribute to the pathogenesis and progression of diseases ranging from cancer, macular degeneration, to chronic inflammation[3]. Growth factors promote neovascularization[4], while cell adhesion molecules (CAMs) are also crucial for vascular morphogenesis[2]. More importantly, signals from growth factors and CAMs crosstalk during vascular morphogenesis[5, 6]. For example, integrin αvβ3 interacts with growth factor receptors and plays complex roles in angiogenesis[6, 7].

Tetraspanins regulate cell adhesion, migration, fusion, and proliferation[8]. Tetraspanin CD82 modulates immune cell activation and viral infection and suppresses tumor progression. In migrating cells, CD82 overexpression inhibits both protrusive and retractive cellular processes by disrupting actin reorganization[9]. CD82 overexpression also alters cell adhesions[9]. At the plasma membrane, CD82 interacts with membrane lipids such as GM2 and modulates membrane lipid composition[10–12]. CD82 inhibits integrins, EGFR, c-Met, and uPAR[9] and reduces downstream signaling of Src, $p130^{CAS}$/Crk, Rho small GTPases, and β-catenin[9]. However, how CD82 regulates cytoskeletal organization and membrane protein activities is still unclear. CD82 is expressed in ECs and arteriolar smooth muscle cells[13–15], but whether it regulates vascular function remains unknown. We found pathological angiogenesis and EC movement were increased in *Cd82 knockout* (KO) mice, likely resulting from the upregulations of CAMs and their initiated signaling. Such upregulations were caused by sequential changes in gangliosides, lipid rafts, CAM-membrane microdomain interactions, and then CAM endocytosis. Hence, CD82 modulates CAM trafficking by preventing lipid raft aggregation and dissociating CAMs from lipid rafts, and CD82-ganglioside-CD44 signaling restrains angiogenesis by inhibiting EC adhesiveness and motility.

Methods

Reagents, PCR, and cellular function assays

Detailed descriptions of reagents, PCR analyses, and cell migration, invasion, sprouting, adhesion, proliferation, and survival assays are listed in Supplement.

Mice and cells

The establishment of *CD82-null* mouse line, mouse genotyping strategy, and isolation of primary ECs are described in Supplement. Animal studies were performed with the approval from the institutional animal care and use committees.

Angiogenesis assays

Detailed descriptions of *in vivo* Matrigel plug, tumor, retina, myocardial infarction (MI) angiogenesis and *ex vivo* aortic ring angiogenesis are listed in Supplement.

Confocal Microscopy, Fluorescence resonance energy transfer (FRET), and Total internal reflection fluorescence microscopy (TIRFM)

See Supplement for details.

Stochastic optical reconstruction microscopy (STORM)

ECs were plated on fibronectin (FN)-coated MatTek dishes for 24 hours, then incubated with Alexa 647-conjugated CTxB for 20 min on ice, washed, and fixed. STORM imaging was performed as described previously[16]. Briefly, image acquisition was performed on a Nikon Eclipse Ti microscope using a 150mW 647nm laser in TIRF mode on continuous illumination. Thirty thousand frames per image were collected at a rate of 50 Hz using a 100× PlanApo 1.45NA Nikon objective projected on an Andor iXon DU897 EMCCD camera. Single molecule fitting and image rendering was performed with N-STORM software within NIS Elements (version AR 4.13.04) with a localization precision of ~40nm.

Endocytosis assay

See Supplement for details.

Statistical analyses

Data are presented as means±SEM or means±SD and were analyzed with JMP pro 11 software (SAS Institute, Cary, NC). The normality of data was examined prior to any test. For two group comparison, two-tailed, unpaired Student's t tests were performed if samples exhibit normal distribution while non-parametric Wilcoxon rank sum test were performed if samples are not normally distributed. For multiple group comparison, Kruskal-Wallis test followed by Dunn tests were performed if Kruskal-Wallis test was significant. Differences are considered significant for p values<0.05.

Results

Endothelial CD82 regulates vascular morphogenesis

To confirm *Cd82* expression in endothelium, we examined CD82 mRNA in murine primary ECs isolated from lung and liver by droplet digital PCR and found *Cd82* was expressed in these ECs. The level of CD82 mRNA was almost three times higher than the level of hypoxanthine-guanine phosphoribosyltransferase (HGPRT), a house-keeping gene (Figure S1A). Also, we used flow cytometry to detect CD82 proteins at the surfaces of human

dermal microvascular ECs (HMECs), umbilical vein ECs (HUVECs), and retinal capillary ECs (HRCECs). We found CD82 was expressed in these human ECs (Figure S1B).

Then, we examined CD82 vascular function using a gene ablation approach. The *Cd82* KO mouse line was generated by using homologous recombination and *Cre-Lox*P deletion strategies (Figure S2A). Since *Cre* is driven by human cytomegalovirus promoter and gene deletion occurs at all cells[17], the deletion of *Cd82* gene was expected to be ubiquitous and was confirmed by Southern blotting and PCR at the DNA level and qRT-PCR at the mRNA level in various tissues (Figure S2B–S2C). For example, using qRT-PCR, we found the levels of the truncated CD82 mRNA in MLECs from *Cd82-null* mice varied from 3% to 6% of the levels of the full-length CD82 mRNA from WT mice (Figure S2D). The *Cd82-null* mice are viable and fertile in C57BL/6 and FVB genetic backgrounds.

To determine the role of CD82 in vascular morphogenesis, we first performed Matrigel plug angiogenesis assay. The Matrigel plugs excised from *Cd82-null* mice exhibited a marked increase in neovascularization, as determined by immunofluorescent and immunohistochemical analyses of CD31 expression (Figure 1A). Vascular area and microvessel density increased by approximately 100% and 130%, respectively, upon *Cd82* ablation. More blood perfusion, which is correlated with functional vessel formation and evidenced by color and hemoglobin content of the Matrigel plugs, was found in *Cd82-null* mice compared to WT mice. Increased lumen formation was proportional to more vasculature in *Cd82-null* group, suggesting CD82 is dispensable for proper tubulogenesis. CD31 staining was always surrounded by and partially colocalized with the staining of pericyte marker NG2, confirming CD31 labels vasculature. Secondly, we examined tumor angiogenesis by subcutaneously implanting syngenic Lewis lung carcinoma cells. In the implanted tumor, angiogenesis was dramatically greater in *Cd82-null* mice than in WT mice (Figure 1B); so does tumor size.

For retinal angiogenesis at P18, by which active angiogenesis is largely completed, WT and *Cd82-null* mice displayed no obvious difference in forming superficial radial and collateral vessels, suggesting CD82 is not required for ultimate development of retina vessels (Figure S3A). For hyperoxia-induced ablation of retinal blood vessels, which leads to an avascular area, no difference was observed between WT and KO groups (Figure S3B). After mice are returned to normoxia, the surge of neovascularization resulted from the vessel ablation forms vessel tufts to alleviate ischemia. The tuft formation was profoundly higher in both number and area in *Cd82-null* mice than in WT mice (Figure 1C), further supporting CD82 preferentially inhibits pathological retinal angiogenesis.

Mycardial infarction (MI) induces active angiogenesis during acute phase. Angiogenesis in the MI regions of *Cd82-null* mice at one week after MI was apparently more pronounced than the one of WT mice (Figure 1D). Importantly, the recovery of cardiac function, reflected by the ejection fraction of left ventricle, was also significantly better in *Cd82-null* than WT group. To substantiate these findings, we examined *ex vivo* ability of aortic artery to undergo angiogenesis. *Cd82-null* aortic rings had greater microvascular sprouting with the length and area of sprouted vessels increasing by approximately 58% and 64%, respectively (Figure 1E). BS1-lectin staining confirmed the sprouts were endothelial.

ECs assemble into capillary networks in 3-dimensional extracellular matrices, which mimics vasculogenesis. We found that the cable network formation was also markedly enhanced in *Cd82-null* MLECs after ECs were seeded in fibrin gel for 2, 8, and 24 h (Figures 1F and S4). Time-lapse videomicroscopy revealed EC migration leading to cable formation was increased in *Cd82-null* ECs than in WT ECs (data not shown).

CD82 mainly alters EC migration and invasion

To address the cellular mechanism by which CD82 restrains pathologic angiogenesis, we assessed the roles of CD82 in EC proliferation and survival. *Cd82* removal slightly promoted EC proliferation and survival (Figure S5).

Because CD82 inhibits cell movement in cancer cells[9], we also examined cell movement. First, significantly greater migration was detected for *Cd82-null* ECs onto FN or LN 111, toward chemoattractants, than for WT ECs (Figure 2A). Second, *in vitro* invasion of ECs through Matrigel was also markedly greater in *Cd82-null* than in WT group (Figure 2B). More importantly, the depth that newly formed vessels penetrate into Matrigel gel plug was much greater in *Cd82-null* than in WT group (Figure 2B), suggesting *Cd82-null* ECs also exhibited higher invasiveness *in vivo*. Third, the penetration distance of ECs from their coated beads in fibrin gel was largely enhanced upon CD82 silencing (Figure 2B). Because mouse ECs hardly attach to the beads, we performed this experiment with HUVECs. Furthermore, markedly more CD82-silenced ECs were found at the tips of endothelial sprouts originated from the beads coated with equal numbers of CD82-silenced and -nonsilenced ECs (Figure 2C), indicating ECs gained invasiveness upon CD82 reduction. Notably, changes in cell migration and invasion are apparently much larger than the ones in cell proliferation and survival.

Because tetraspanins regulate microextrusion morphogenesis and microextrusions may modulate cell movement[18], we examined microextrusion in ECs. Compared to WT ECs, *Cd82-null* ECs formed more and developed longer CD31- and CD44-containing microextrusions (Figure 2D), supporting CD82 inhibits microextrusion morphogenesis.

During retinal angiogenesis, tip cells and their filopodia were markedly increased at P5 in *Cd82-null* retinas, compared to WT ones (Figure S3C), strongly suggesting more invasive and robust vessels are developed during angiogenesis in *Cd82-ablated* mice.

Since CD82 associates with CAMs, we examined cell-matrix adhesion. *Cd82-null* MLECs showed marked increases in adhesion onto hyaluronan (HA) and laminin (LN) 111 but no change onto FN (Figure 2E).

CD82 inhibits cell surface presence of endothelial CAMs

To determine how CD82 regulates EC motility and adhesiveness, we examined the effect of *Cd82* ablation on EC surface expressions of tetraspanins and CAMs by using flow cytometry. Tetraspanin CD9, integrin α6, integrin αV, and CD44 were upregulated in *Cd82-null* ECs, while others remained equivalent between two groups (Figure 3A). Because CD44 associates with tetraspanins and plays roles in EC motility and angiogenesis[19–22], we compared CD44 protein and mRNA levels in WT and *Cd82-null* ECs and found total CD44

proteins became increased upon *Cd82* ablation (Figure 3B) but CD44 mRNA remained unchanged (Figure 3C). Similarly, the upregulated surface level of integrin α6 was not accompanied by an increase in integrin α6 mRNA level either (Figure 3C). These observations suggest the increases in CD44 and integrin α6 protein levels upon *Cd82* ablation were not a result of altered gene transcription but were due to changes in protein turnover. Such a conclusion is consistent with no correlations in gene expression between CD82 and CD44 or integrin α6 in endothelia, although a reverse correlation exists between CD82 and integrin αV genes (Figure S6).

EC adhesion onto HA, a matrix ligand of CD44, was enhanced without CD82(Figure 2E), reflecting an increase of functional CD44 proteins. Also, CD44 was upregulated in the vessels of the Matrigel plug implanted in *Cd82-null* mice (Figure 3D). Moreover, CD44 mAb reduced aortic ring angiogenesis and endothelial network formation of *Cd82-null* ECs to the WT level (Figures 3E–3F and S7). Furthermore, CD44 mAb inhibited EC migration and brought down the migration of *Cd82-null* ECs to the level of WT ECs (Figure 3G).

To substantiate this finding, we examined CD44 expression in MI-induced angiogenesis (Figure S8A). In the heart tissue from normal rats, CD44 expression was negligible in capillary within myocardium, indicating CD44 is minimally expressed in quiescent microvessels. At the first and second weeks after MI, massive angiogenesis was accompanied by drastic increase of endothelial CD44. At the fourth week after MI, CD44 expression was significantly reduced in ECs within the MI areas that underwent fibrosis. Thus, CD44 expression in ECs is correlated with angiogenesis. The same conclusion can be reached during the angiogenesis following MI in WT and *Cd82-null* mice (Figure S8B)

CD82 restrains cytoskeletal connection and signaling of CAMs

The changes in CAMs drove us to investigate their cytoskeletal connection. In *Cd82-null* ECs, tetraspanins CD9 and CD81 were localized in focal complex-like structures at the cell periphery (Figure 4A). Integrin β1 exhibited unaltered distribution but formed more focal adhesions in *CD82-null* ECs (Figure 4B). Higher staining intensities of integrin α6 and CD44 were found in *CD82-null* ECs, but their global cellular distributions appeared to be unchanged (Figure 4B–4C).

Focal adhesion formation and development was markedly enhanced in *Cd82-null* ECs, based on the staining of talin, a marker of nascent focal adhesion, and paxillin and vinculin, constituents of focal adhesion (Figure 4D).

FAK/Src-p130^{CAS}/Crk signaling is regulated by CAMs and tetraspanins and controls cell movement[2, 9]. The protein level and auto-activation (pY^{397}) of FAK remained unchanged but full activation of FAK (pY^{577}) was elevated in *Cd82-null* ECs (Figure 4E). Tyr^{410}-phosphorylated p130^{CAS} and Tyr^{416}-phosphorylated c-Src were markedly greater upon *Cd82-ablation*, indicating an upregulated FAK/Src-p130^{CAS} signaling axis.

PI3K-Akt signaling, denoted by Ser^{473}-phosphorylated Akt, was upregulated in *Cd82-null* ECs (Figure 4F). ERM proteins (Figure 4G), which link tetrapsanins and CD44 to actin

cytoskeleton, and VEGFR-2(Figure 4H), which triggers angiogenic signaling, remained unaltered.

CD82 modulates CD44 endocytosis and lipid raft clustering

Since tetraspanins regulate endocytosis[8, 9], more CAMs at *Cd82-null* EC surface may result from less endocytosis. Indeed, absolute amounts of the internalized CD9 and CD44 were lower in *Cd82-null* MLECs than in WT MLECs, after 60-min endocytosis (Figures 5A and S9A). After normalization to their levels at the cell surface, CD9 and CD44 internalization dropped further in KO group. In contrast, the endocytosis of CD81 and integrin α5, the levels of which weren't altered upon *Cd82* ablation, was equivalent between two groups. Earlier studies showed CD44 is internalized through clathrin-independent endocytosis pathway (CLIC)[23, 24]. Using GM1, a cargo of CLIC route, as tracer, we found most internalized CD44 proteins colocalized with GM1 in both groups after 2- and 5-min endocytosis (Figures 5B and S9B), suggesting *Cd82* ablation didn't alter the endocytosis route of CD44. However, CD44 and GM1 internalizations were substantially reduced after 5-min endocytosis in *Cd82-null* ECs (Figure 5B–5C), suggesting clathrin-independent endocytosis of CD44 and this endocytic pathway *per se* were both inhibited without CD82.

Since CD82 overexpression alters the interaction between tetraspanin-enriched microdomains (TEMs) and lipid rafts[12], we analyzed the distributions of CD44, TEM marker CD9, and lipid raft marker GM1 at EC basal surface with TIRFM. CD44 distributions were similar in a majority of ECs (Figure 6A) but displayed a clustered pattern in approximately one third of *Cd82-null* ECs (the middle image). CD9 exhibited similar staining characteristics at the basal surface between two groups. Notably, GM1-positive lipid rafts were evenly distributed to large extent in fixed WT cells but became clustered much more often to form small patches in fixed KO cells. Using super-resolution imaging, we confirmed GM1 frequently formed clusters with sizes of approximately 30~50 nm at the basal surface of *Cd82-null* ECs. Normalized Ripley's K function [L(r)-r] determines whether a given pattern is clustered, random, or dispersed[25]. Positive humps in the normalized curves indicated clustering over those distances. *Cd82-null* ECs displayed significant clustering of GM1 over short distances compared to WT cells. Latrunculin dispersed CD44 and GM1 clusters (Figure S10), suggesting actin involvement in clustering and excluding GM1 clusters as post-fixation artifacts.

We then examined the colocalizations of CD44 with TEM and lipid raft markers at the basal section (a ~230 nm-thick focal plane) of fixed MLECs with confocal microscopy (Figures 6B and S11). The colocalizations of CD44 with GM1- or flotillin-positive lipid rafts and CD9-positive TEMs were significantly increased in *Cd82-null* ECs (Table 1), suggesting more CD44 are coalescent with TEMs and rafts.

Using fluorescent probes C_{16}DiI and C_{16}DiO, which incorporate to lipid ordered regions at the plasma membrane[26], we found the FRET signal from C_{16}DiI and C_{16}DiO (Figure S12) was drastically elevated in *Cd82-null* ECs and such elevation could be abrogated by raft disrupter filipin (Figure 6C), suggesting higher order of lipid rafts in *Cd82-null* EC membrane. Consistently, the surface levels of gangliosides GM1, GM2, and GM3 were

upregulated in *Cd82-null* ECs (Figure 6D). Ceramide and cholesterol levels remained unaltered.

Detergent solubility of CAMs and tetraspanin was reduced upon *Cd82* ablation even after cytoskeletal disruption (Figure S13), suggesting CD82 mainly modulates membrane compartmentalization of these proteins (Supplemental Results). Since in TEMs CD82 associates with tetraspanins and CAMs[9], we analyzed TEMs through immunoprecipitation profiles (Figure 6E). CD9 and CD9-associated unknown surface proteins (X1 and X2), not CD9-associated integrins and CD81, were increased in *Cd82-null* ECs, suggesting extra CD9 proteins at EC surface are integrin- and CD81-free. Levels and species of the surface proteins associated with β1 integrins and CD44 were generally unchanged upon *Cd82* ablation, despite of CD44 upregulation. Thus, integrin-CD9 association and CD44 complex, not CD9-containing TEM, remain unaltered without CD82.

To confirm the roles of lipid raft clustering and ganglioside increase in angiogenesis, we examined the effects of filipin and PDMP, a glucosylceramide synathase inhibitor which blocks ganglioside formation, on aortic ring angiogenesis and EC motility. Filipin and PDMP diminished the difference in angiogenesis between WT and KO groups and reduced *Cd82-null* EC cell motility to the WT level (Figure 6F–6G).

CD82-ganglioside-CD44 signaling and pathological angiogenesis

Increased angiogenic potential in *Cd82-null* mice makes us to question whether CD82 is downregulated during pathological neovascularization. Indeed, vascular expression of CD82 was largely diminished in proliferative diabetic retinas, which is caused by profound angiogenesis, compared to CD82 expression in the vessels of normal retina (Figure S14). Moreover, we compared vascular expressions of CD82 in human normal breast and breast cancer tissues using tissue microarray and found CD82 proteins in the blood vessels within invasive breast cancer were reduced, compared to those in normal breast tissue (Figure 7A, arrowheads). While vascular CD44 exhibited a converse pattern, indicating reduced CD82 and enhanced CD44 coexist in human tumor angiogenesis. The same changes in CD82 and CD44 expressions were also observed from epithelial to tumor cells.

Our study reveals CD82-ganglioside-CD44 signaling is connected to angiogenic potential (Figure 7B). We perturbed this signaling *in vivo* to confirm its importance. By administration of PDMP or CD44 shRNA in Matrigel plug angiogenesis assay, the increased angiogenesis in *Cd82-null* group was reduced to the levels of WT group (Figure 7B), indicating increased gangliosides and CD44 are essential for the enhanced angiogenesis *in vivo* upon *Cd82* ablation.

Discussion

Herein we identified the confinements of EC movement and angiogenic potential as novel functions for CD82, demonstrated that lipid raft clustering and CAM trafficking modulate angiogenic potential, and revealed a novel mechanistic paradigm that membrane glycosphingolipids tune angiogenic potential through altering CAM at the plasma membrane. Since no gross vascular abnormality was observed after development, CD82

likely restrains EC movement to suppress angiogenesis under pathological conditions and prevent excessive vascular morphogenesis under physiological conditions. Also, our study conceptualizes the schemes that 1) membrane protein regulates lipid rafts and 2) membrane compartmentalization of CAMs modulates EC movement. To inhibit EC movement, CD82 likely enhances CAM endocytosis by changing CAM-membrane microdomain interactions. Without CD82, higher magnitudes of CAMs and CAM-initiated signaling at EC surface more efficiently induce focal adhesive structures and microextrusions, drive EC movement, and subsequently facilitate pathological angiogenesis (Figure S15).

CD82 confines angiogenesis by mainly restraining EC movement

Although CD82 is expressed in ECs[27] and *Cd82-null* mice exhibit elevated vascular morphogenic potential, these mice do not display obvious vascular defects, suggesting that CD82 is not essential for physiological vessel development. However, it is unlikely to have developmental vascular defects when vascular morphogenic potential is above normal. Also, increased vascular morphogenesis is not needed for normal development of animals. Increased pathological angiogenesis in *Cd82-null* mice underlines that 1) loss of CD82 function cannot be mitigated or compensated after development and 2) CD82 inhibits molecular and cellular events unique to or critical for pathological angiogenesis, which is distinct from physiological angiogenesis[28]. Our observations highlight that pathological angiogenesis lacks efficient regulatory mechanism for EC movement, which is the main cellular event that CD82 controls during angiogenesis, and suggest that downregulating EC movement serves a therapeutic strategy selectively against pathological angiogenesis.

Pathological angiogenesis is characterized by its morphogenic simplicity[29]. In *Cd82-null* mice, the increased angiogenic potential is associated with more rapid and efficient formation of capillaries, driven mainly by enhanced EC movement. In other words, the relative simplistic morphogenic program of pathological angiogenesis depends more on EC movement than significantly more complex physiological angiogenesis does. Notably, angiogenesis without CD82 is functional, as evidenced by better blood-perfused Matrigel plug, larger size of tumor, more perfused vascular tufts, and stronger cardiac function after MI in *Cd82-null* mice.

CD82 restrains EC movement by inhibiting CAMs

CD82-dependent alteration in cell adhesion is likely to be directly responsible for the change in movement. For example, enhanced adhesion onto HA promotes EC infiltration in interstitial tissue while upregulated FAK/Src-p130^{CAS} and Akt activities serve as pro-migratory signaling in *Cd82-null* ECs.

Tetraspanins preferentially associate with LN-binding integrins like α6 integrins. The upregulated α6 integrins correlate with the enhanced *Cd82-null* EC adhesion onto LN111. Interestingly, the upregulated αV integrins and unchanged α5β1 integrin, both are RGD-binding integrins, did not enhance *Cd82-null* EC adhesion onto FN. Hence whether CD82 affects integrin activation remains to be determined. Alternatively, the upregulated α6 and αV integrins may contribute to other activities such as Notch and Netrin signaling[30, 31]. To visualize how CD82, CD44, and integrin are related at the molecular level, we cross-

referenced the top 20 genes most frequently co-transcribed with CD82 with their known protein-protein interactions (Figure S16). Most of the four known protein-protein interactions shared by CD82 and CD44 are associated with cell migration and angiogenesis, suggesting potential genetic partners by which the two may exert their phenotype-altering influence.

CD44 and tetraspanins activate multiple signaling pathways[8, 32]. FAK/Src-p130^{CAS} and Akt signaling affect cell adhesion and movement and is altered upon CD82 overexpression[8, 9]. CD44 partitions to lipid rafts and associates with Src through its cytoplasmic domain[33, 34]. The increased FAK/Src-p130^{CAS} activity in *Cd82-null* ECs likely results from the elevated levels and/or altered microdomain coalescences of CAMs like CD44 at the plasma membrane. Higher Akt activity could also be caused by more surface CAMs because HA–CD44 binding activates PI-3 kinase-Akt signaling[32]. Src is likely situated between CD44 and Akt since Src indirectly activates PI-3 kinase and Akt during angiogenesis[35], and also Src maximally activates FAK through FAK-Y^{577} phosphorylation. We propose CD82 trans-dominantly inhibits CD44 and its downstream signaling by modulating the membrane microdomain coalescence of CD44, to confine EC-HA adhesion. Consistently, CD44 has proangiogenic properties, evidenced by the observations that vascular morphogenesis becomes attenuated in *Cd44-null* mice, CD44 Abs inhibit EC proliferation and vascular morphogenesis, and CD44v6 serves as a coreceptor for c-Met and VEGFR2 in ECs during angiogenesis[19, 22, 36–38]. Our study further revealed how CD44 promotes angiogenesis at molecular level.

CD82 inhibits CAMs by altering the microdomain coalescence and then endocytosis of CAMs

CD44 perturbation reduced the enhanced migration and angiogenesis of *Cd82-null* group to the levels of WT, supporting the notion that CD44 has immediate and major functional connections to CD82. Reductions were also found in WT group, suggesting that CD44 also controls these events at physiological conditions.

The increased expressions of CD44, integrin α6, CD9, and gangliosides at *Cd82-null* EC surface likely result from their decreased turnover at the plasma membrane. Less endocytosis of CD44 apparently causes more CD44 at *Cd82-null* EC surface. Since cholesterol is important for clathrin-independent/CLIC endocytic pathway[39, 40], CD82 modulates this pathway probably by reorganizing saturated lipids into or between membrane microdomains[12]. Increased gangliosides in *Cd82-null* EC plasma membrane likely facilitate 1) lipid raft clustering in a cholesterol-dependent manner, as found in the model membrane[41], and 2) coalescence of CD44 to TEMs and lipid rafts, as tetraspanins physically interact with CD44 and gangliosides[11, 42]. We predict microdomain reorganization leads to less endocytosis of microdomain residents such as CD44, CD9, and gangliosides.

Stronger cell-matrix adhesiveness and greater focal adhesive structures in *Cd82-null* ECs reflect robust membrane–cytoskeleton connection, which may reduce CAM endocytosis. But increased interactions of CD44 with lipid rafts and TEMs likely play more dominant roles in its trafficking, as CD44 is internalized through clathrin-independent, raft-dependent pathway[23, 24].

CD82 is a lipid raft organizer

Robust microextrusions in *Cd82-null* ECs likely result from the reorganized membrane microdomains and contribute to active motile behaviors and strong adhesiveness during angiogenesis, given that microextrusions may modulate cell adhesion and movement[18]. Tetraspanins hadn't been found in focal complex and adhesion[8], the membrane microdomains of cytoskeleton-connected CAM clusters. Upon *Cd82* ablation, redistribution of tetraspanins/TEMs to focal complexes further corroborates CD82 as a membrane domain organizer. Because TEMs contain various CAMs, such redistribution suggests greater clustering of CAMs and stronger EC adhesion strengthening.

CD82-ganglioside-CD44 signaling in angiogenesis

Ganglioside buildup upon *Cd82* removal and subsequent lipid raft clustering upregulate CD44 in pathological angiogenesis, which can be attenuated by inhibiting CD82-ganglioside-CD44 signaling. Although filipin could exert a broader effect on cells, the notion that filipin inhibits angiogenesis by disrupting lipid rafts is supported by the effects of ganglioside reduction and CD44 blockade.

Our study revealed that membrane microdomain landscape plays a key role in pathological angiogenesis and delineated that CD82 modulates CAM trafficking and then surface expression by altering lipid rafts clustering (Figure S14). Importantly, we first demonstrated that CD82 protein drives lipid raft reorganization. Because angiogenesis is linked to many diseases, our observations have far reaching implications. Future studies will determine how CD82 alters membrane lipids and evaluate the therapeutic potentials of CD82-ganglioside-CD44 signaling against pathological angiogenesis. Studies on CD82 and tumor progression have so far focused on the metastasis-suppressive effect that CD82 exerts directly on tumor cells[9]. Given that endothelial CD82 inhibits tumor angiogenesis, CD82 can be a drug candidate with dual benefits against tumor progression.

Supplementary Material

Refer to Web version on PubMed Central for supplementary material.

Acknowledgements

XAZ is an Oklahoma TSET Cancer Research Scholar. We thank Drs. S. Vesely, Y. Chen, S. Frank, R. McEver, L. Xia, H. Chen, C. Griffin, and K. Kyler for discussion, Dr. X. Qi for technical support, and OMRF imaging facility for confocal microscopy.

Funding Sources: This study was funded by a NIH grant CA096991 and AHA grant 13GRNT17040028 to XAZ.

References

1. Hanahan D. Signaling vascular morphogenesis and maintenance. Science. 1997; 277:48–50. [PubMed: 9229772]
2. Avraamides CJ, Garmy-Susini B, Varner JA. Integrins in angiogenesis and lymphangiogenesis. Nat Rev Cancer. 2008; 8:604–617. [PubMed: 18497750]
3. Carmeliet P. Angiogenesis in health and disease. Nat Med. 2003; 9:653–660. [PubMed: 12778163]
4. Olsson AK, Dimberg A, Kreuger J, Claesson-Welsh L. Vegf receptor signalling - in control of vascular function. Nat Rev Mol Cell Biol. 2006; 7:359–371. [PubMed: 16633338]

5. Davis GE, Senger DR. Endothelial extracellular matrix: Biosynthesis, remodeling, and functions during vascular morphogenesis and neovessel stabilization. Circ Res. 2005; 97:1093–1107. [PubMed: 16306453]
6. Hodivala-Dilke K. Alphavbeta3 integrin and angiogenesis: A moody integrin in a changing environment. Curr Opin Cell Biol. 2008; 20:514–519. [PubMed: 18638550]
7. Somanath PR, Malinin NL, Byzova TV. Cooperation between integrin alphavbeta3 and vegfr2 in angiogenesis. Angiogenesis. 2009; 12:177–185. [PubMed: 19267251]
8. Yanez-Mo M, Barreiro O, Gordon-Alonso M, Sala-Valdes M, Sanchez-Madrid F. Tetraspanin-enriched microdomains: A functional unit in cell plasma membranes. Trends Cell Biol. 2009; 19:434–446. [PubMed: 19709882]
9. Richardson MM, Jennings LK, Zhang XA. Tetraspanins and tumor progression. Clin Exp Metastasis. 2011; 28:261–270. [PubMed: 21184145]
10. Odintsova E, Butters TD, Monti E, Sprong H, van Meer G, Berditchevski F. Gangliosides play an important role in the organization of cd82-enriched microdomains. Biochem J. 2006; 400:315–325. [PubMed: 16859490]
11. Todeschini AR, Dos Santos JN, Handa K, Hakomori SI. Ganglioside gm2-tetraspanin cd82 complex inhibits met and its cross-talk with integrins, providing a basis for control of cell motility through glycosynapse. J Biol Chem. 2007; 282:8123–8133. [PubMed: 17215249]
12. Xu C, Zhang YH, Thangavel M, Richardson MM, Liu L, Zhou B, Zheng Y, Ostrom RS, Zhang XA. Cd82 endocytosis and cholesterol-dependent reorganization of tetraspanin webs and lipid rafts. FASEB J. 2009; 23:3273–3288. [PubMed: 19497983]
13. Custer MC, Risinger JI, Hoover S, Simpson RM, Patterson T, Barrett JC. Characterization of an antibody that can detect the kai1/cd82 murine metastasis suppressor. Prostate. 2006; 66:567–577. [PubMed: 16372335]
14. Hashimoto A, Tarner IH, Bohle RM, Gaumann A, Manetti M, Distler O, Steinmeyer J, Ulfgren AK, Schulz A, Gay S, Muller-Ladner U, Neumann E. Analysis of vascular gene expression in arthritic synovium by laser-mediated microdissection. Arthritis Rheum. 2007; 56:1094–1105. [PubMed: 17393418]
15. Nagao K, Oka K. Hif-2 directly activates cd82 gene expression in endothelial cells. Biochem Biophys Res Commun. 2011; 407:260–265. [PubMed: 21382346]
16. Roy NH, Chan J, Lambele M, Thali M. Clustering and mobility of hiv-1 env at viral assembly sites predict its propensity to induce cell-cell fusion. J Virol. 2013; 87:7516–7525. [PubMed: 23637402]
17. Schwenk F, Baron U, Rajewsky K. A cre-transgenic mouse strain for the ubiquitous deletion of loxp-flanked gene segments including deletion in germ cells. Nucleic Acids Res. 1995; 23:5080–5081. [PubMed: 8559668]
18. Zhang XA, Huang C. Tetraspanins and cell membrane tubular structures. Cell Mol Life Sci. 2012; 69:2843–2852. [PubMed: 22450717]
19. Cao G, Savani RC, Fehrenbach M, Lyons C, Zhang L, Coukos G, Delisser HM. Involvement of endothelial cd44 during in vivo angiogenesis. Am J Pathol. 2006; 169:325–336. [PubMed: 16816384]
20. Golshani R, Lopez L, Estrella V, Kramer M, Iida N, Lokeshwar VB. Hyaluronic acid synthase-1 expression regulates bladder cancer growth, invasion, and angiogenesis through cd44. Cancer Res. 2008; 68:483–491. [PubMed: 18199543]
21. Savani RC, Cao G, Pooler PM, Zaman A, Zhou Z, DeLisser HM. Differential involvement of the hyaluronan (ha) receptors cd44 and receptor for ha-mediated motility in endothelial cell function and angiogenesis. J Biol Chem. 2001; 276:36770–36778. [PubMed: 11448954]
22. Tremmel M, Matzke A, Albrecht I, Laib AM, Olaku V, Ballmer-Hofer K, Christofori G, Heroult M, Augustin HG, Ponta H, Orian-Rousseau V. A cd44v6 peptide reveals a role of cd44 in vegfr-2 signaling and angiogenesis. Blood. 2009; 114:5236–5244. [PubMed: 19773544]
23. Howes MT, Kirkham M, Riches J, McMahon H, Robinson PJ, Hancock JF, Mayor S, Parton RG. Clathrin-independent carriers form a high capacity endocytic sorting system at the leading edge of migrating cells. J Cell Biol. 2010; 190:675–691. [PubMed: 20713605]

24. Tammi R, Rilla K, Pienimaki JP, MacCallum DK, Hogg M, Luukkonen M, Hascall VC, Tammi M. Hyaluronan enters keratinocytes by a novel endocytic route for catabolism. J Biol Chem. 2001; 276:35111–35122. [PubMed: 11451952]
25. Kiskowski MA, Hancock JF, Kenworthy AK. On the use of ripley's k-function and its derivatives to analyze domain size. Biophys J. 2009; 97:1095–1103. [PubMed: 19686657]
26. Chichili GR, Cail RC, Rodgers W. Cytoskeletal modulation of lipid interactions regulates lck kinase activity. J Biol Chem. 2012; 287:24186–24194. [PubMed: 22613726]
27. Jameson SA, Natarajan A, Cool J, DeFalco T, Maatouk DM, Mork L, Munger SC, Capel B. Temporal transcriptional profiling of somatic and germ cells reveals biased lineage priming of sexual fate in the fetal mouse gonad. PLoS Genet. 2012; 8:e1002575. [PubMed: 22438826]
28. Jain RK. Molecular regulation of vessel maturation. Nat Med. 2003; 9:685–693. [PubMed: 12778167]
29. Nagy JA, Dvorak AM, Dvorak HF. Vegf-a and the induction of pathological angiogenesis. Ann Rev Pathol. 2007; 2:251–275. [PubMed: 18039100]
30. Estrach S, Cailleteau L, Franco CA, Gerhardt H, Stefani C, Lemichez E, Gagnoux-Palacios L, Meneguzzi G, Mettouchi A. Laminin-binding integrins induce dll4 expression and notch signaling in endothelial cells. Circ Res. 2011; 109:172–182. [PubMed: 21474814]
31. Larrieu-Lahargue F, Welm AL, Thomas KR, Li DY. Netrin-4 activates endothelial integrin {alpha}6{beta}1. Circ Res. 2011; 109:770–774. [PubMed: 21799154]
32. Zoller M. Cd44: Can a cancer-initiating cell profit from an abundantly expressed molecule? Nat Rev Cancer. 2011; 11:254–267. [PubMed: 21390059]
33. Bourguignon LY, Zhu H, Shao L, Chen YW. Cd44 interaction with c-src kinase promotes cortactin-mediated cytoskeleton function and hyaluronic acid-dependent ovarian tumor cell migration. J Biol Chem. 2001; 276:7327–7336. [PubMed: 11084024]
34. Oliferenko S, Paiha K, Harder T, Gerke V, Schwarzler C, Schwarz H, Beug H, Gunthert U, Huber LA. Analysis of cd44-containing lipid rafts: Recruitment of annexin ii and stabilization by the actin cytoskeleton. J Cell Biol. 1999; 146:843–854. [PubMed: 10459018]
35. Kumar P, Amin MA, Harlow LA, Polverini PJ, Koch AE. Src and phosphatidylinositol 3-kinase mediate soluble e-selectin-induced angiogenesis. Blood. 2003; 101:3960–3968. [PubMed: 12522014]
36. Griffioen AW, Coenen MJ, Damen CA, Hellwig SM, van Weering DH, Vooys W, Blijham GH, Groenewegen G. Cd44 is involved in tumor angiogenesis; an activation antigen on human endothelial cells. Blood. 1997; 90:1150–1159. [PubMed: 9242547]
37. Trochon V, Mabilat C, Bertrand P, Legrand Y, Smadja-Joffe F, Soria C, Delpech B, Lu H. Evidence of involvement of cd44 in endothelial cell proliferation, migration and angiogenesis in vitro. Int J Cancer. 1996; 66:664–668. [PubMed: 8647630]
38. Yu Q, Stamenkovic I. Cell surface-localized matrix metalloproteinase-9 proteolytically activates tgf-beta and promotes tumor invasion and angiogenesis. Genes Dev. 2000; 14:163–176. [PubMed: 10652271]
39. Damm EM, Pelkmans L, Kartenbeck J, Mezzacasa A, Kurzchalia T, Helenius A. Clathrinand caveolin-1-independent endocytosis: Entry of simian virus 40 into cells devoid of caveolae. J Cell Biol. 2005; 168:477–488. [PubMed: 15668298]
40. Sabharanjak S, Sharma P, Parton RG, Mayor S. Gpi-anchored proteins are delivered to recycling endosomes via a distinct cdc42-regulated, clathrin-independent pinocytic pathway. Dev Cell. 2002; 2:411–423. [PubMed: 11970892]
41. Lingwood D, Ries J, Schwille P, Simons K. Plasma membranes are poised for activation of raft phase coalescence at physiological temperature. Proc Natl Acad Sci U S A. 2008; 105:10005–10010. [PubMed: 18621689]
42. Mitsuzuka K, Handa K, Satoh M, Arai Y, Hakomori S. A specific microdomain ("glycosynapse 3") controls phenotypic conversion and reversion of bladder cancer cells through gm3-mediated interaction of alpha3beta1 integrin with cd9. J Biol Chem. 2005; 280:35545–35553. [PubMed: 16103120]

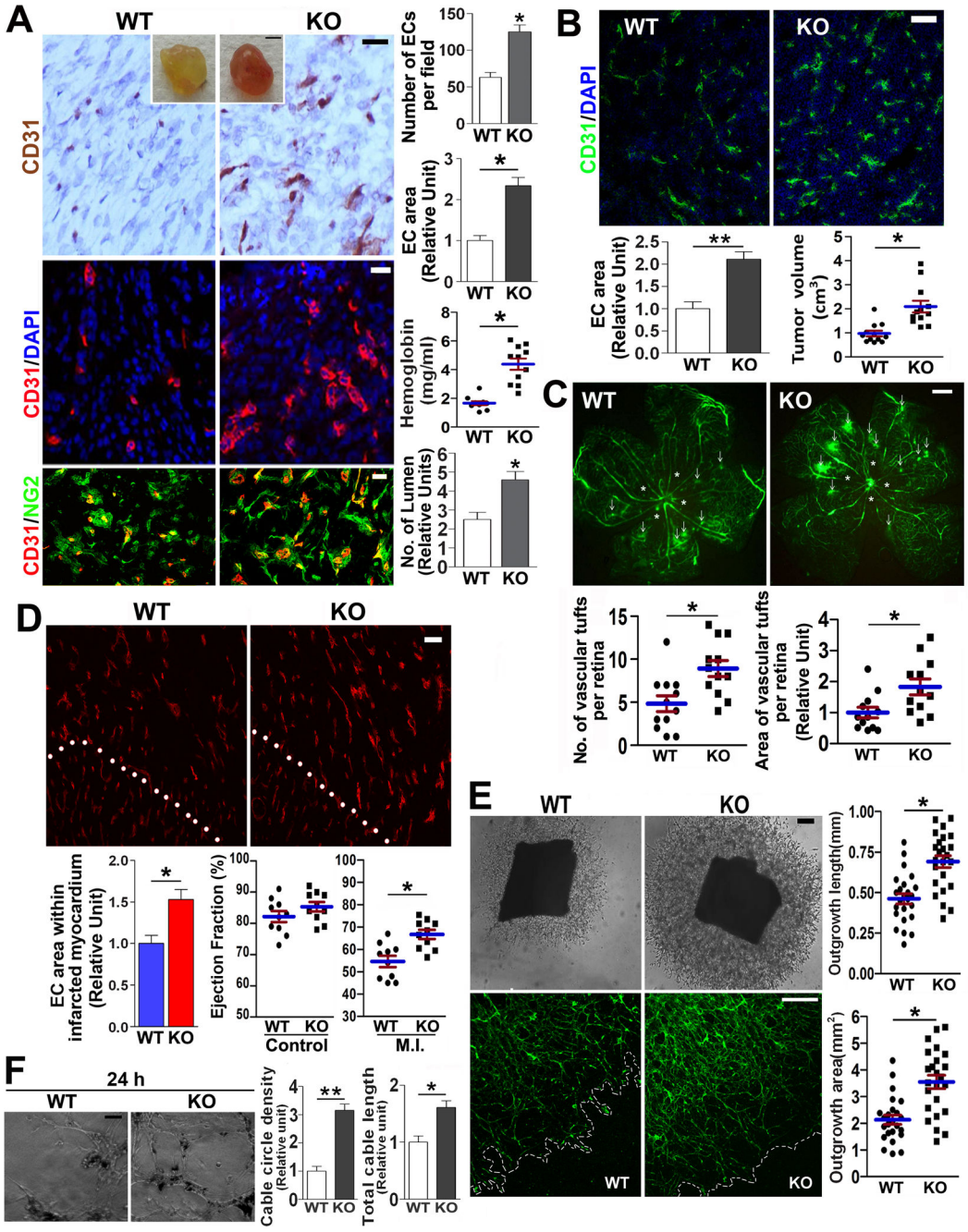

Figure 1.

Vascular morphogenesis is enhanced upon *Cd82* ablation. (**A**) Matrigel plug angiogenesis. Matrigel plugs were harvested after 7-day implantation (Scale bar, 0.5 cm), sectioned, and stained with CD31 for immunohistochemistry (brown; scale bar, 0.2 mm) and immunofluorescence (red; scale bar, 0.1 mm). The sections were co-stained with DAPI (blue) for nucleus or NG2 Ab (green) for pericytes. Angiogenesis was quantified by either counting CD31-positive cells per microscopic field for immunohistochemistry or measuring CD31-staining area for immunofluorescence with Image J software. CD31-positve, ring-like

structures were counted as lumen. Hemoglobin was detected using Drabkin reagent. (**B**) Tumor angiogenesis. Cryosections of LLC tumors were co-stained with CD31 Ab (green) and DAPI (blue) or CD31(green) Abs. Vascular areas within tumors were quantified as described above, and tumor sizes were measured by (length×width^2)/2. Scale bar, 20μm. (**C**) Angiogenesis during oxygen-induced retinopathy. Retinas were isolated and flat-mounted. Angiography images were captured. Arrowheads denote tufts, and asterisks indicate avascular areas. Scale bar, 500 μm. The numbers (left panel) and areas (right panel) of retinal tufts were quantified. (**D**) MI-induced angiogenesis. Mice were euthanized at 1 week after MI, and frozen sections of heart were immunostained with CD31 mAb and photographed. White dotted lines denote the borders of MI border zone (upper right) and normal myocardium (lower left) areas. CD31-staining areas were quantified with Image J software. Ejection fractions of left ventricles were measured by echocardiography at 1 week after MI. Scale bar, 20μm. (**E**) Aortic ring angiogenesis. Mouse thoracic aortic rings were cultured within Matrigel for 5 days. Shown are phase-contrast microscopic images of branching vessel-like structures and fluorescent microscopic images of the structures stained with BS1-lectin-FITC. Scale bars, 0.2 mm. Lengths and areas of the vessel-like structures from aortic rings were quantified. (**F**) *In vitro* vasculogenesis. MLECs were seeded in fibrin gel and photographed at 24 h. Scale bar, 0.2 mm. EC cable circle density and EC cable length were quantified. Quantitative results in this figure are presented as mean±SEM (n=3~5 independent experiments, *, $P<0.05$, **, $P<0.01$)..

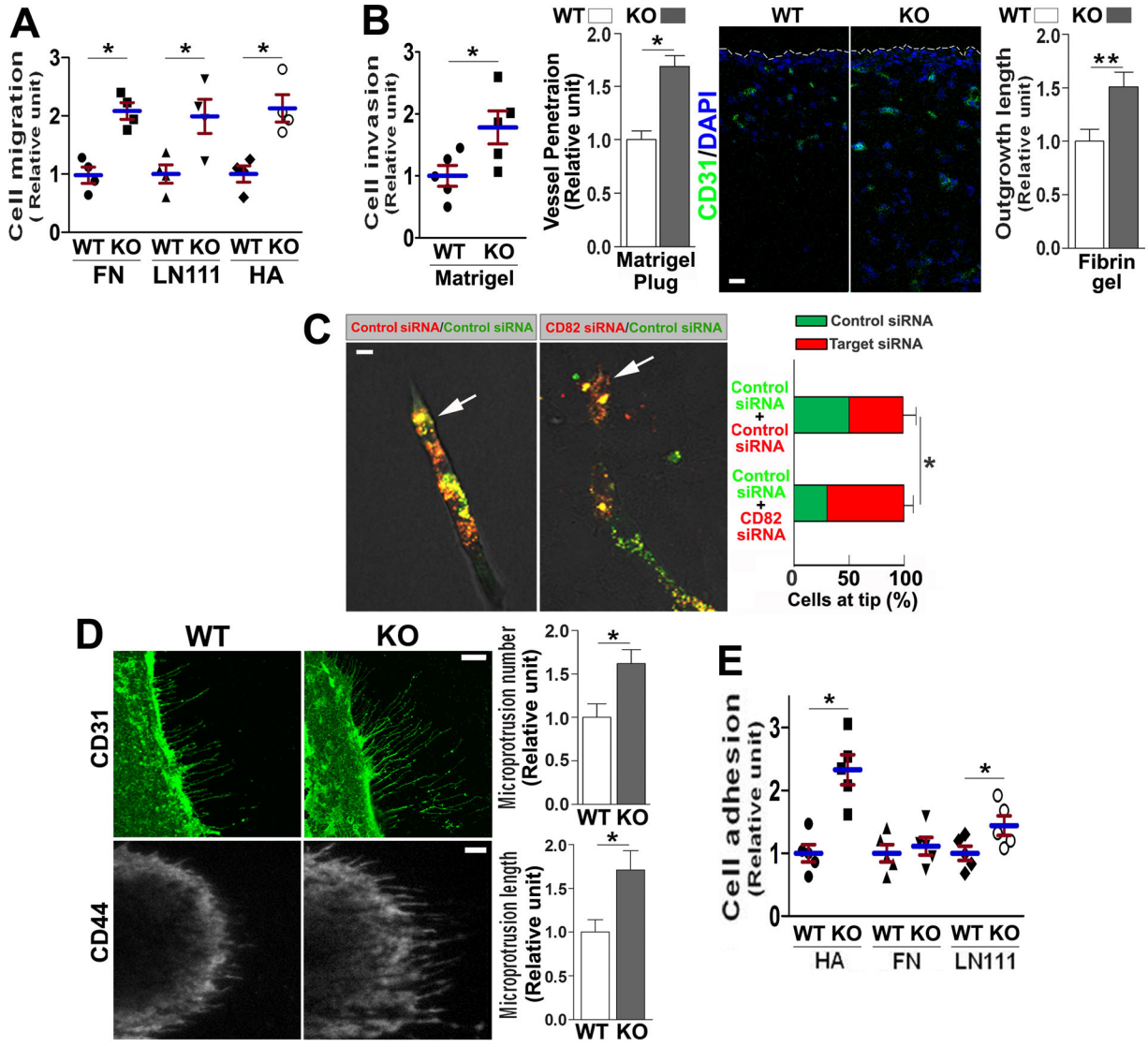

Figure 2.

Motility and adhesiveness of WT and *Cd82-null* ECs. (**A**) Cell migration. MLEC migration onto FN (10 μg/mL), LN111(10 μg/mL), or HA (200 μg/mL) was assayed for 6 h, then the cells that migrated onto the bottom side of the filter were counted, and the data are reported as relative migration units.. (**B**) Cell invasion. For solitary invasion, MLECs that invaded through Matrigel (0.33 mg/mL) in Transwell inserts were quantified. EC invasion *in vivo* was evaluated in Matrigel plug angiogenesis assay, and the distance of CD31 staining between the plug edge and vessel frontier was measured and presented as relative units. Scale bar, 0.1 mm. For collective invasion, HUVECs were coated on beads, placed in fibrin gel, and allowed to sprout in the presence of mitomycin for 48 h. The average lengths of EC outgrowth from beads into fibrin gel were quantified. (**C**) ECs at sprout tips. The siRNA-transfected, PKH26 or PKH67 dye-labeled HUVECs were coated on beads and cultured in fibrin gel for 48 h. Green or red ECs at sprout tips were quantified. Arrows indicate tip cells. (**D**) Microextrusion morphogenesis. MLECs were immunofluorescently stained for CD31 or CD44 and photographed by confocal microscopy or TIRFM, respectively. Numbers of

microextrusions per cell were counted, and lengths of microextrusions were measured with Image J software. In each experiment, 10 ECs per group were quantified. Scale bars, 10 μM. (**E**) Cell–matrix adhesion. MLECs were seeded in the wells coated with FN (10 μg/mL), LN111(20 μg/mL), or HA (200 μg/mL) in triplicate and incubated at 37°C in 5%CO_2 for 35 min. Non-adherent ECs were then removed by gentle washes, and the adhered ECs were counted and presented as relative adhesion unit. Quantitative results in this figure are presented as mean±SEM (n=3~5 independent experiments; *, $P<0.05$; **, $P<0.01$).

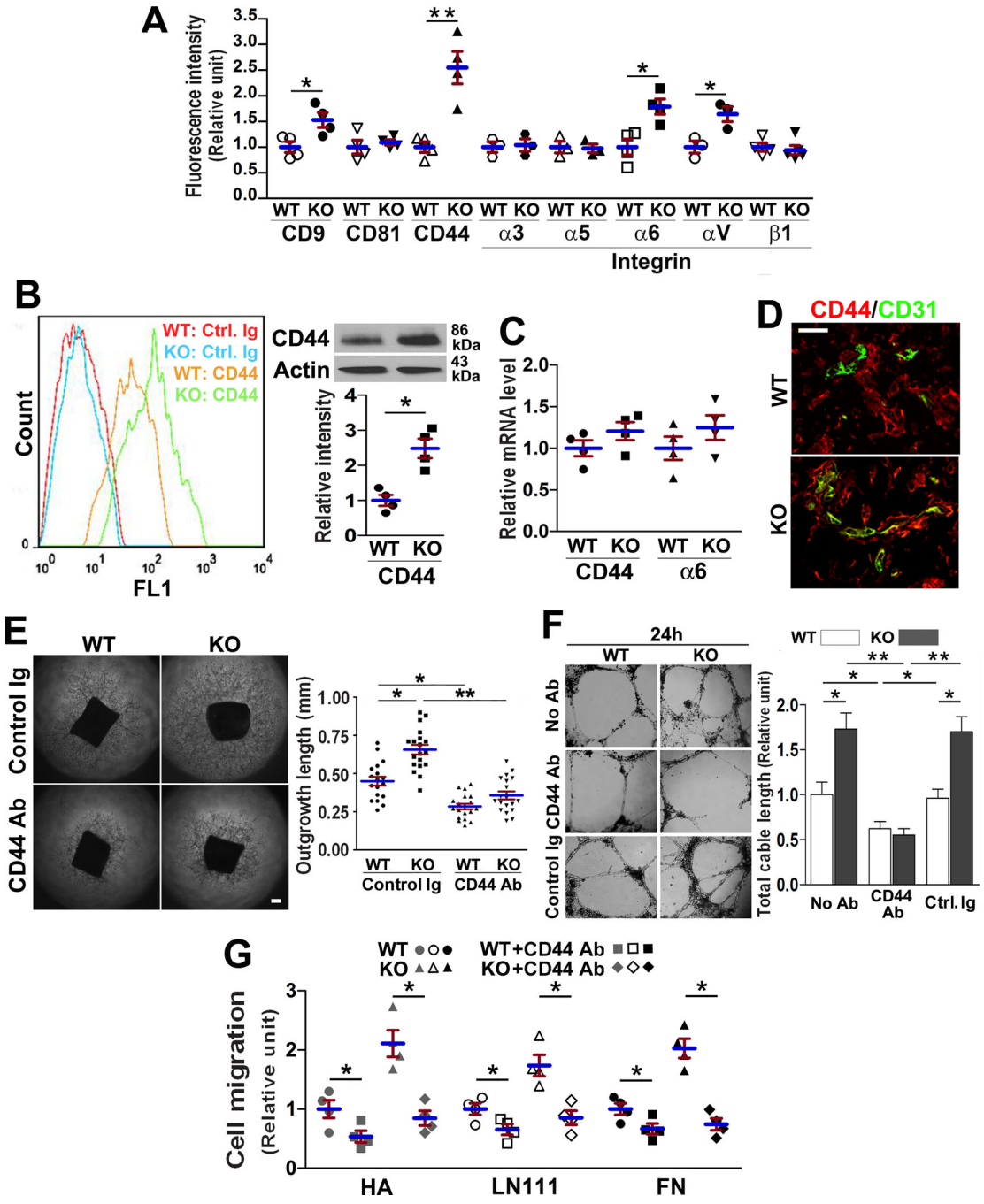

Figure 3.

CD82 regulates CD44 level and functions. (**A**) Flow cytometric analysis of the surface levels of various CAMs on MLECs (**B**) Cell surface and total cellular CD44 proteins from MLECs were measured by flow cytometry and Western blot with CD44 mAb KM114, respectively. CD44 bands were quantified by densitometry and normalized to β-actin signals. (**C**) CD44 and integrin α6 mRNAs were measured by qRT-PCR. (**D**) CD44 expression during angiogenesis. Cryosections of implanted Matrigel plugs from angiogenesis assay were co-stained with CD44(red) and CD31(green) mAbs. Scale bar, 100

μm. Aortic ring angiogenesis (**E**) and MLEC cable network formation in 3D-matrix (**F**) were assayed with CD44 mAb KM114 or control IgG (20μg/ml). EC networks were imaged at 24 h after seeding. Scale bars, 0.2 mm. (**G**) The effect of CD44 mAb KM114 (20μg/ml) on MLEC migration onto FN (10μg/ml), LN111 (10μg/ml), or HA (200μg/ml). All quantitative data in this figure are presented as mean±SEM (n=4 independent experiments; *, $P<0.05$; **, $P<0.01$).

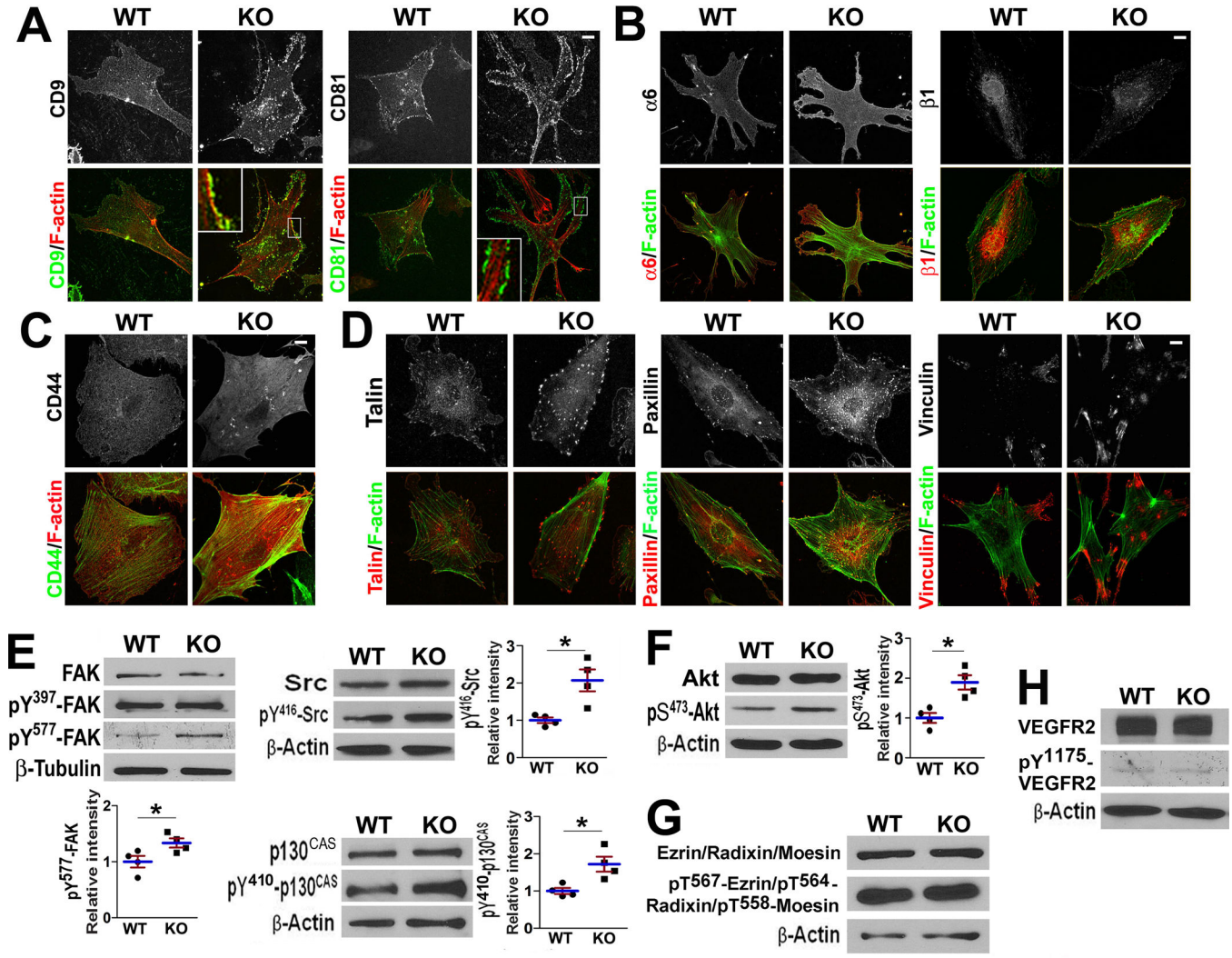

Figure 4.

CD82 restrains CAM-related cellular structures and signaling. (**A**–**D**) After 2-day culture on FN, MLECs were fixed, permeabilized, and incubated with CD9 mAb (KMC8) or CD81 mAb (EAT-2)(**A**), integrin α6 mAb (Goh3) or integrin β1 mAb (9EG7)(**B**), CD44 mAb (KM114)(**C**), and vinculin, paxillin, or talin mAb (**D**), followed by incubation with fluorochrome-conjugated secondary Ab and phalloidin. Images were acquired with confocal microscopy. (**E**–**H**) MLECs were cultured on gelatin-coated plates for 2 days, serum-starved in some experiments, and then lysed in 1% NP-40. Lysates were probed with Abs to total and activated Src, FAK, and p130^{CAS} (**E**), Akt (**F**), ERM proteins (**G**), and VEGF-R2 (**H**). Band densities were normalized with the one of β-actin or β-tubulin (mean±SD; n=3~5; *: P<0.05).

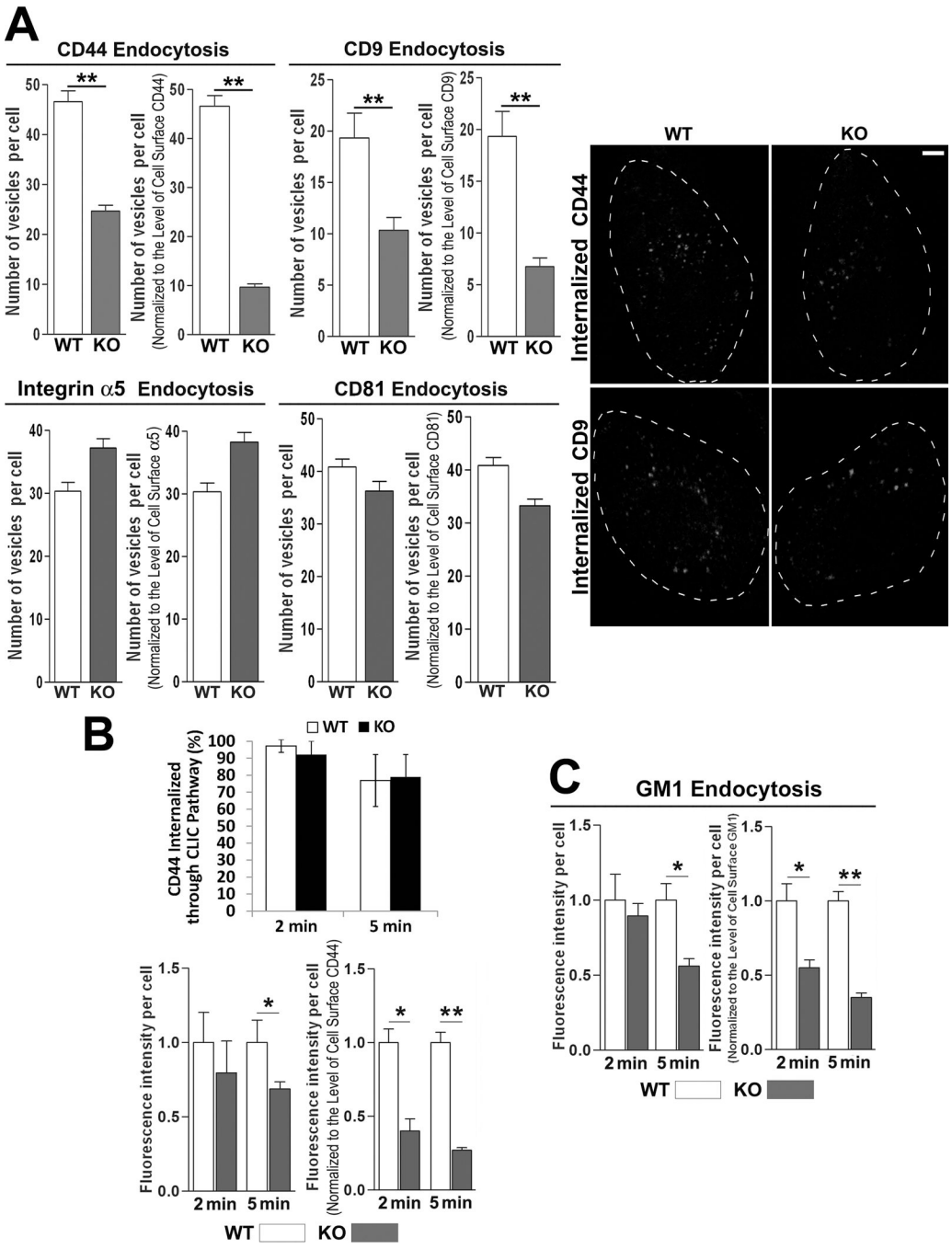

Figure 5.

CD82 facilitates clathrin-independent endocytosis of CD44. (**A**) CD44, CD9, CD81, and integrin α5 endocytosis were examined for 1 h by Ab uptake assay using CD44 mAb (KM114), CD9 mAb (KMC8), CD81 mAb (EAT-2), or integrin α5 mAb, respectively. (**B**) and (**C**). Short-term (2 and 5 min) endocytosis of CD44 and GM1 were examined in MLECs with fluorescently labeled CD44 mAb and CTxB, respectively, by confocal microscopy. Endocytosis was quantified by either counting fluorescent vesicles or measuring fluorescent

intensity (mean±SEM; n=3~5 independent experiments; *P<0.05, **P<0.01). Scale bar: 10 μm.

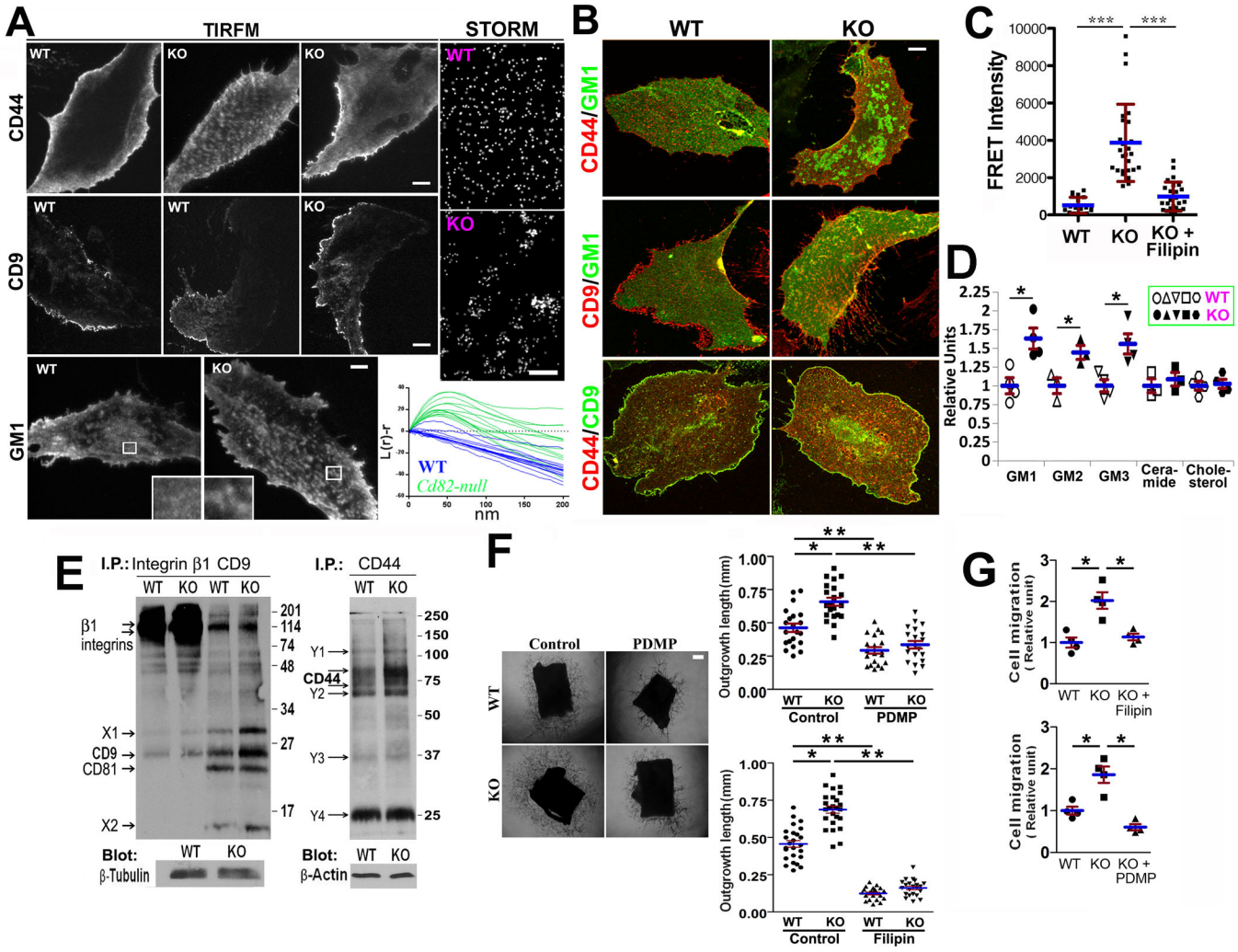

Figure 6.

CD82 modulates CAM distribution at the EC–matrix interface and membrane microdomain organization. (**A**) The distributions of CD44, CD9, and GM1 at the EC–matrix interface. TIRFM analyses were performed on the fixed MLECs, which were stained with either CD44 mAb (KM114) and then FITC-conjugated secondary Ab, Alexa488-conjugated CD9 mAb (KMC8), or Alexa488-conjugated CTxB. Bar, 10 μm. STORM analyses were performed on the fixed MLECs stained with Alexa647-conjugated CTxB. Bar, 85 nm. L(r)-r curves for WT (blue) and *Cd82-null* (green) GM1 staining were generated based on the analysis of 14 fields for WT cells and 13 for *Cd82-null* cells, respectively. (**B**) Co-localizations of CD44, CD9, and GM1 at the EC basal surface. MLECs were cultured in complete medium on FN-coated coverslips for 2 days, fixed, permeabilized, and incubated with fluorochrome-conjugated CTxB, CD9 mAb, or CD44 mAb. Images of EC basal focal plane (~230 nm thickness) were captured with confocal microscopy. Bar, 10 μm. (**C**) FRET analysis was performed in ECs, and relative FRET intensity was calculated as described in “Methods”. Some *Cd82-null* ECs were treated with filipin (5μg/ml) at 37°C for 30 min prior to FRET analysis. (**D**) Flow cytometry analyses of GMs, ceramide, and cholesterol at MLEC surface using GM Abs, ceramide Ab, and filipin, respectively. (**E**) MLECs were labeled with Sulfo-

NHS-LC-Biotin and lysed in 1% Briji-97. Immunoprecipitations were performed with CD44 mAb (IM7), β1 integrin mAb (9EG7), or CD9 mAb (KMC8). Identities of the cell surface proteins associated with integrin β1 or CD9, marked as "X" or “Y”, remain unknown. (**F**) (**G**) In the presence or absence of filipin (10μg/ml) or PDMP (50μM), aortic ring angiogenesis assay was performed in Matrigel (**F**) and Transwell cell migration was assayed onto FN (**G**). Outgrowth lengths of the vascular sprouts from thoracic aortic rings were quantified and the ECs migrated onto bottom side were counted. Bar, 0.2 mm. Quantitative data in this figure are presented as mean±SEM (n=3~5 independent experiments; *:$P<0.05$; **:$P<0.01$; ***:$P<0.001$).

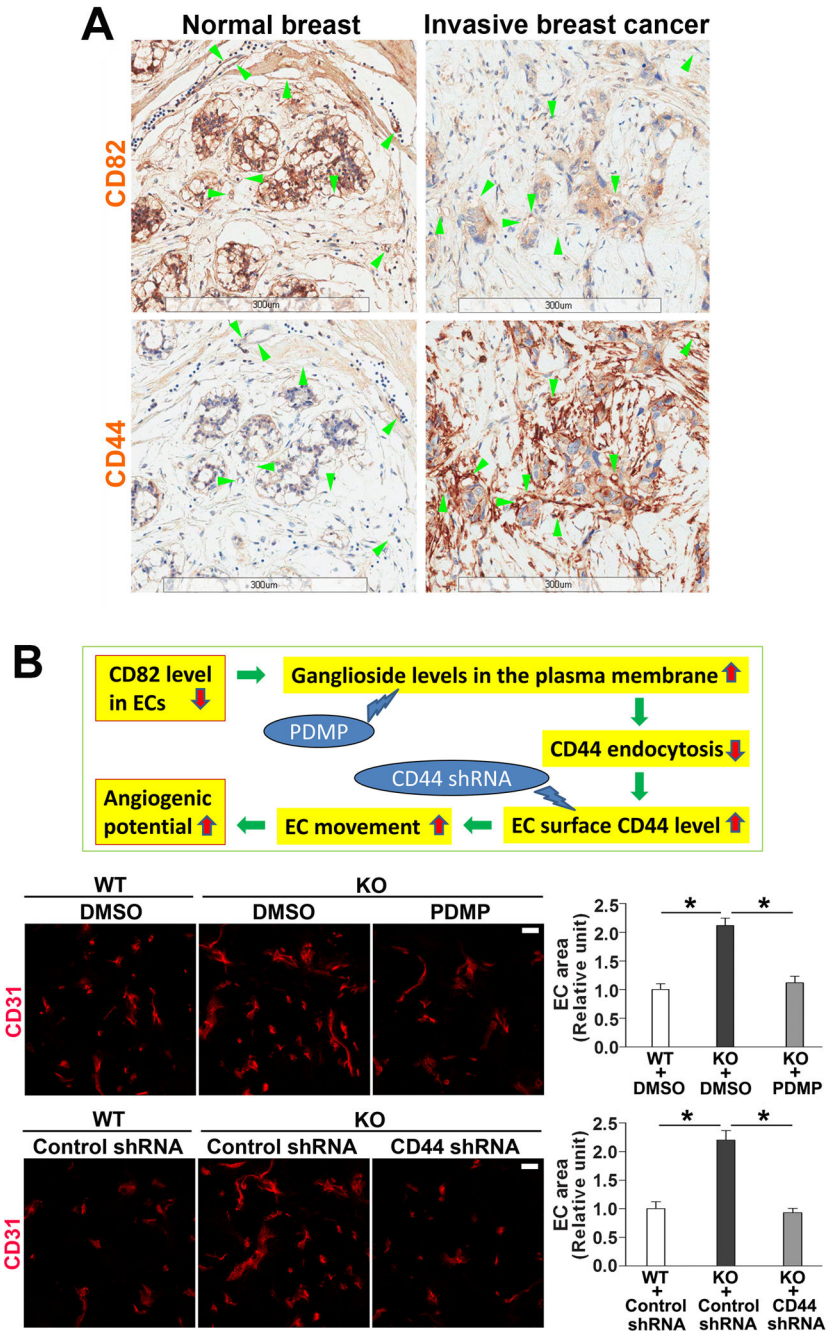

Figure 7.

CD82-ganglioside-CD44 signaling regulates pathological angiogenesis. (**A**) Changes in CD82 and CD44 expressions in human tumor angiogenesis. Human normal breast and invasive breast cancer tissues were stained with CD44 or CD82 mAb (brown), and the sections were imaged by Aperio Scanscope. (**B**) Effects of ganglioside reduction and CD44 silencing on angiogenesis *in vivo*. The rationale for perturbing CD82-gangliosides-CD44 signaling is presented in the scheme. After PDMP or CD44 shRNA lentiviruses was mixed with Matrigel to a final concentration of 50 μM or 1×10^6 particles per ml of Matrigel,

respectively, Matrigel plug angiogenesis was performed and quantified as described in Figure 1A. CD31-staining areas are shown as mean±SEM (n=4; *: $P<0.05$). Scale bar, 20 μm.

Table 1

Colocalization of CD44, CD9, and GM1 at and near EC basal surface

	Pearson		Mander		M1		M2	
	WT	**KO**	**WT**	**KO**	**WT**	**KO**	**WT**	**KO**
CD44&GM1	0.31±0.20	0.46±0.18*	0.38±0.20	0.53±0.17*	0.56±0.21	0.76±0.18*	0.39±0.26	0.49±0.22
CD44&Flotilin	0.44±0.06	0.56±0.10**	0.52±0.08	0.62±0.12*	0.51±0.06	0.68±0.14**	0.79±0.13	0.78±0.13
CD44&CD9	0.32±0.10	0.38±0.06*	0.38±0.11	0.46±0.08*	0.44±0.16	0.53±0.12*	0.30±0.14	0.43±0.10**
CD9&GM1	0.24±0.13	0.25±0.11	0.29±0.15	0.31±0.11	0.51±0.17	0.52±0.14	0.27±0.13	0.27±0.21

Pearson: Pearson's correlation coefficient; Mander: Mander's overlap coefficient; M1: Mander's coefficient M1(green channel); M2; Mander's coefficient M2(red channel);

mean±SD; N=3~4;

*: P<0.05;

**: P<0.01.